Coastal Engineering 79 (2013) 42–56

Contents lists available at SciVerse ScienceDirect

Coastal Engineering

journal homepage: www.elsevier.com/locate/coastaleng

Experimental study of bore-driven swash hydrodynamics on permeable rough slopes

G.A. Kikkert [a,*], D. Pokrajac [b], T. O'Donoghue [b], K. Steenhauer [b]

[a] Department of Civil and Environmental Engineering, School of Engineering, Hong Kong University of Science and Technology, Hong Kong
[b] School of Engineering, King's College, University of Aberdeen, Aberdeen, AB24 3UE, United Kingdom

ARTICLE INFO

Article history:
Received 5 November 2012
Received in revised form 17 April 2013
Accepted 22 April 2013
Available online 21 May 2013

Keywords:
Dam-break
Experimental data
Infiltration
Permeability
Swash
Tsunami

ABSTRACT

A detailed experimental investigation of the hydrodynamics of large-scale, bore-driven swash on steep permeable, rough beaches is described. The experiments were carried out on two permeable, but fixed rough beaches, made of 1.3 mm sand and 8.4 mm gravel, respectively. The large-scale discrete swash event was produced by the collapse of a dam break-generated bore on the beach. Simultaneous depths and velocities were measured using laser-induced fluorescence (LIF), and particle image velocimetry (PIV), respectively. Depth time series, instantaneous velocity profiles, depth-averaged velocities, instantaneous turbulent kinetic energy profiles, depth-averaged turbulent kinetic energy, turbulent shear stress profiles and bed shear stresses are presented for several cross-shore measurement locations in the swash. The effect of beach permeability is investigated by comparing new experimental results with previously published data for impermeable beaches with identical surface roughness (Kikkert et al., 2012). The detailed data can be used to test and develop advanced numerical models for bore-driven swash on rough permeable beaches.

1. Introduction

The swash zone is considered to be the most dynamic region of the beach and considerable research effort has been devoted to studying it. The majority of field studies have investigated the swash zone on sandy beaches focusing on the hydrodynamics (e.g., Baldock and Hughes, 2006; Conley and Griffin, 2004; Hughes, 1992; Raubenheimer, 2002) or the sediment transport (e.g., Blenkinsopp et al., 2011; Horn and Mason, 1994; Hughes et al., 1997; Masselink and Hughes, 1998; Masselink and Russell, 2006; Puleo et al., 2000). Field studies on gravel beaches include Austin and Masselink (2006) and Masselink et al. (2010). The field-based investigations have resulted in a reasonable understanding of the main characteristics of the swash zone processes (Butt and Russell, 2000; Elfrink and Baldock, 2002; Masselink and Puleo, 2006). However, more detailed research is required in order to fully understand the key fundamental processes governing hydrodynamics and sediment transport in the swash zone. One of the key processes is the infiltration of water into the beach.

Detailed data sets are usually collected in laboratory experiments, because research carried out in the laboratory enables greater control over the beach conditions. The majority of laboratory studies reported in the literature involve impermeable immobile beds (e.g., Barnes et al., 2009; Kikkert et al., 2012; Petti and Longo, 2001; Shin and Cox, 2006). Lara et al. (2006) created a permeable, fixed bed using wire boxes filled with gravel (nominal diameter of 19 mm or 39 mm) to study the effect of permeability on the hydrodynamics, but the focus of their measurements was on the surf zone, not the swash zone. Other measurements on permeable beaches usually involve mobile sediment (e.g., Pedrozo-Acuña et al., 2006) so that the effects of permeability cannot be separated from the effects of sediment mobility. To the authors' best knowledge no investigations have been carried out on permeable fixed beaches, and focussed solely on the effects of beach permeability on swash hydrodynamics.

The present paper reports new experiments designed to study the detailed hydrodynamics of large-scale bore-driven swash on steep permeable beaches. Experiments were performed on two relatively coarse-grained beaches with different permeability and surface roughness. A detailed description of the subsurface processes recorded in these experiments is reported in Steenhauer et al. (2011). The effect of permeability is investigated by a comparison of the new results with the previously reported results of Kikkert et al. (2012) obtained on impermeable slopes with identical surface roughness and slope.

The paper is organised as follows. Section 2 describes the experimental set-up and measurement. Section 3 presents the experimental results: volume balance for the whole beach, shoreline position, flow depth, depth-averaged velocity and velocity profiles are presented first, followed by results for turbulent kinetic energy, Reynolds stress, bed shear stress and friction factors. The main conclusions of the study are presented in Section 4.

* Corresponding author. Tel.: +852 2358 8190.
E-mail address: kikkert@ust.hk (G.A. Kikkert).

0378-3839
http://dx.doi.org/10.1016/j.coastaleng.2013.04.008

2. Experimental setup

The experimental setup used to carry out the permeable bed experiments is very similar to the setup used for the impermeable bed experiments of Kikkert et al. (2012). This section therefore highlights only the additional elements of the setup required for the permeable beach experiments.

2.1. Facility

The experiments were carried out in the Fluid Mechanics Laboratory at the University of Aberdeen. A water reservoir was placed inside an existing 20 m long, 0.9 m high and 0.45 m wide wave flume (Fig. 1). The reservoir was fronted by a gate that was raised at high speed (~4 m/s). The initial water depth in the reservoir (h_d) was 600 mm and the initial water depth in front of the beach (h_0) was 62 mm (Fig. 1). With ratio h_d / h_0 of approximately 0.1, raising the gate generated a plunging breaker (Stansby et al., 1998) leading to a bore approximately 0.25 m high with velocity in the order of 2.0 m/s. The bore propagated towards the 1:10 sloped beach located approximately 4.2 m downstream. The beach consisted of sediment throughout its depth. The initial ground water level within the beach was also h_0. This level was controlled by a weir placed 0.5 m beyond the end of the beach.

Experiments were carried out with two different sediments, coarse sand and gravel, with nominal sediment size 1.3 mm and 8.4 mm respectively. Steenhauer et al. (2011) reported the Forchheimer coefficients for both sediments, which show that the gravel is more permeable than the sand by an order of magnitude. The effect of packing on the homogeneity of the sand was minimised by compacting the sediment in the flume under water. A perforated plate at the end of the beach (10.8 m from gate) stopped the sediment from collapsing but still allowed an unobstructed flow of water out of the beach. To create an immobile beach the top 30 mm of the beach was cemented using a dilute water–cement mixture (3% cement by weight, Steenhauer et al., 2011). Separate tests confirmed that, up to the range of the experimental error, the permeability of the sediments was not changed by cementing (Steenhauer et al., 2011). The final beach level was within 1–2 mm of the desired 1:10 slope.

2.2. Instrumentation, measurements and analysis

The origin of the $x - z$ coordinate system is at the intersection between the initial water level and the top of the roughness elements of the beach (Fig. 1). This point is referred to as the initial shore-line location and is 0.623 m from the toe of the beach and 4.82 m from the gate. The x-axis is parallel to the beach slope and positive shoreward, while the z-axis is perpendicular to the slope. The moment that the gate of the reservoir is raised is defined as $t = 0$. Simultaneous velocity and depth measurements were recorded, centred on 6 cross-shore locations at x = -1.802 m, 0.072 m, 0.772 m, 1.567 m, 2.377 m and 3.177 m for the sand beach. For the gravel beach the swash excursion did not reach x = 3.177 m, so no measurements were recorded at this location.

Velocities were measured using cross-correlation particle image velocimetry (PIV) and flow depths were measured using laser induced fluorescence (LIF) (Sue et al., 2006). Neutrally buoyant particles (titanium-coated hollow glass particles with a mean diameter of 20 μm) and fluorescent dye with a concentration of approximately 0.1 mg/l were added to the flow and illuminated using a New Wave Solo III Nd YAG Laser. The laser sheet was introduced to the centre of the flow from below the flume, through highly polished 20 mm thick Perspex PIV towers that extended from the bottom of the flume to the beach face. The reflected laser light from the particles and the emitted light from the fluorescent dye were captured by two digital video cameras that were rotated to be aligned with the 1:10 slope of the beach. The PIV camera was rotated slightly backwards to eliminate interference by the free surface when flow depths were small while the LIF camera was rotated forwards so that the camera view was at all times above the free surface. The PIV and LIF systems were combined into a single PIV–LIF system controlled and synchronised by Dantec Dynamics Studio v1.45 software, enabling the velocity and flow depth to be recorded simultaneously at 13.5 Hz. The system was triggered at the moment when the gate was raised. The instantaneous velocity vector fields had a spatial resolution between 1 and 2.5 mm and a random error of 5 to 15 mm/s. The flow depth had an error of approximately 1 pixel, giving instantaneous depth data with a spatial resolution and random error of 0.1 to 0.3 mm.

In addition to the combined PIV–LIF measurements at the 6 locations, a second set of LIF-only measurements was carried out to measure the swash lens, i.e., the instantaneous surface water profile over the whole of the swash extent. For these measurements the Laser was positioned above the flume and illuminated approximately 300 mm of the cross-shore extent of the lens. The complete lens was measured by combining measurements from approximately 12 cross-shore locations (the exact number depended on the maximum run-up).

Repeatability of swash events using the rig was excellent (Kikkert et al., 2012), which meant that measurements from many repeats of the same event could be used to obtain representative ensemble-averages and turbulence measurements. To ensure identical conditions for all repeated runs, water that infiltrated into the beach in the previous run was allowed to drain from the beach. The time required to recover the initial groundwater level was determined by recording the change in water level in the saturated area of the beach prior, during and after a single swash run (Steenhauer et al., 2011). The recovery period for the sand and gravel beach was 60 min and 6 min respectively. Due to the relatively long recovery time, fewer repeats of individual swash events were carried out for the sand beach than for the gravel beach. For the simultaneous PIV/LIF depth and velocity measurements, swash events were repeated 50 times for the gravel beach and 15 times for the sand beach. For the LIF-only measurements of swash depth, experiments were repeated 10 times for the gravel beach and 8 times for the sand beach.

3. Experimental results and discussion

3.1. Surface/subsurface exchange across beach surface

Steenhauer et al. (2011) provide a detailed description of the processes occurring within a permeable beach while the bore climbs its surface. Water infiltrates into the initially unsaturated beach and forms a wetting front, which travels towards the groundwater level.

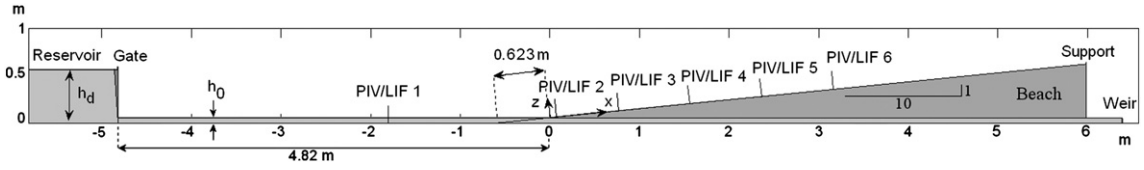

Fig. 1. Permeable bed set-up, initial conditions and PIV/LIF locations.

The air within the beach gets trapped between the wetting front and the groundwater, so its pressure increases. The pore-air pressure build-up is larger within the less permeable sand beach. Increased pressure below the wetting front decreases the water flux across the beach surface until eventually, at some locations, it becomes zero. Close to the initial shoreline, the pressure increases most rapidly, causing reverse movement of water, i.e., exfiltration, which begins almost immediately after the bore arrival and lasts throughout the duration of the swash event. The corresponding exfiltration rates, though non-zero, are very small because the volume of water that infiltrates the beach during the very brief period following bore arrival is very small. At the same locations close to the initial shoreline air was also observed to escape the subsurface. The gravel beach is much more permeable so the wetting front moves much faster. In addition, since air below the wetting front can escape more easily, the pore-air pressure builds up at a much smaller rate, and the wetting front reaches the groundwater level very soon after the bore arrival. From this moment the beach becomes saturated and further infiltration into the beach is significantly reduced.

Infiltration of water into the permeable beach reduces the volume of water left on the beach. The infiltration discharge across the total beach surface at any point in time, Q_{inf}, is evaluated as:

$$Q_{\mathrm{inf}}(t) = Q_{\mathrm{inf}low}(t) - Q_{st}(t) = \overline{h}(x_0,t)\overline{\langle u\rangle}(x_0,t) - \frac{1}{2\Delta t}\left[\int_{x_0}^{\infty}\overline{h}(x,t+\Delta t)dx - \int_{x_0}^{\infty}\overline{h}(x,t-\Delta t)dx\right] \quad (1)$$

where Q_{inflow} is the amount of water that travelled through the cross-section at $x_0 = 0.072$ m (with $Q_{inflow} < 0$ indicating a seaward flux), Q_{st} is the storage within the surface water, h is flow depth, u is the streamwise velocity, Δt is the time step for the velocity measurements, and an overbar and square brackets indicate ensemble-average and depth-average, respectively. The results for Q_{st} were smoothed using a 3-point moving-average routine in order to reduce the noise resulting from the evaluation of time derivatives. Time series of Q_{inflow}, Q_{st} and Q_{inf} are shown in Fig. 2. Just after bore arrival the infiltration discharge across the gravel beach surface, Q_{inf}, is higher than across the less permeable sand beach surface. For both beaches Q_{inf} reaches its maximum relatively soon after bore arrival on the beach, and then starts to decrease due to decreasing vertical hydraulic gradients. Gradually decreasing infiltration rate is a well-known feature of infiltration from a surface layer into a dry porous material. Here it is enhanced by the buildup of pressure within the subsurface, which is especially pronounced in the sand beach. The water flux across the sand beach surface becomes close to zero at approximately 7.3 s, when the pressure within the beach has become sufficiently high to balance the weight of both surface and subsurface water. It is important to note that the pressure buildup in the subsurface may have been higher, and therefore the infiltration rates lower, than may be expected for an equivalent beach in the field. The two-dimensional nature of the experimental setup meant that air could only move in a shoreward direction. In the field, air is also able to move in a direction along the beach and hence may escape laterally due to alongshore non-uniformity of the incident bore and beach slope. In the gravel beach the lower region of the beach becomes saturated relatively quickly, and this further decreases the infiltration discharge. At $t =$ 6.3 s, the gravel beach becomes saturated at all locations under the surface flow, and the water flux across the beach surface is negligible.

Integrating the time series of Q_{inflow} and Q_{inf} over the duration of the swash event gives an estimate for the total volume of water that travelled through the cross section at $x_0 = 0.072$ m and the total volume infiltrated into the beach, respectively. (For the purpose of this calculation the infiltration discharge is assumed to increase linearly between time of bore arrival and the first point in time that Q_{inflow} could be obtained.) The total inflow volumes of water for the sand and the gravel beach were 0.30 m^3/m and 0.27 m^3/m respectively. The total volume of water that infiltrated into the beach by the end of the swash cycle is 0.10 m^3/m for the sand beach, with 70% occurring during uprush. For the gravel beach it was 0.14 m^3/m (90% during uprush). This means that the percentage of water lost from the surface flow was 33% and 52% for the sand and the gravel beach respectively.

3.2. Shoreline position

The effect of the permeability on the run-up can be observed in Fig. 3, which presents the shoreline position time series for the two permeable beaches and also for their impermeable beach counterparts. The shoreline is defined as that point where the flow depth, measured from the top of the roughness elements in the bed-normal direction, is equal to 5 mm. Consider first the permeable gravel beach. The trajectory of the shoreline is similar to the impermeable gravel beach for approximately 0.5 s after the bore arrives at the initial shoreline location. During this period infiltration into the beach is too

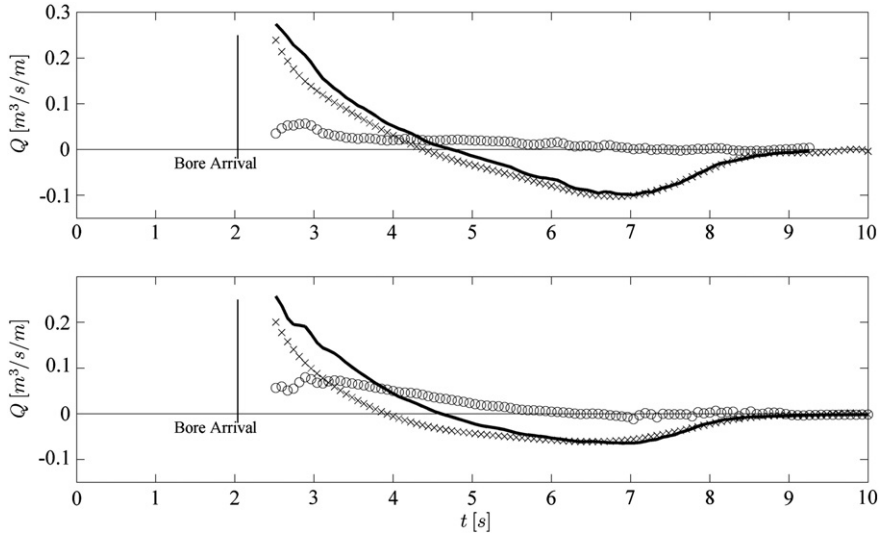

Fig. 2. Flow discharge at x = 0.072 m (Q_{inflow}) (−), change in volume of surface water on the entire beach per unit time (Q_{st}) (x), and infiltration into the subsurface across the whole beach surface (Q_{inf}) (o) for sand (top) and gravel beaches (bottom). All quantities are expressed as volume per unit time and unit width of flume.

small to affect the shoreline movement. Later on the infiltration rate increases, and this slows down the propagation of the shoreline compared to the impermeable beach. Initially, this reduction is small, but it increases quickly, until at 4.4 s, the infiltration discharge just behind the shoreline becomes equal to the surface flow discharge approaching the shoreline, so that the shoreline itself stops moving up the beach, i.e., the maximum run-up has been reached. The maximum run-up is much smaller than on the impermeable beach (3.0 m, compared to 4.0 m), and it occurs earlier (4.4 s compared to 5.5 s). Furthermore, flow reversal does not occur as soon as the maximum run-up is reached. This can be seen from the flow reversal times (based on the bed-parallel depth-averaged velocity) which are also shown in Fig. 3. There is a considerable lag between the time of the maximum run-up ($t = 4.4$ s) and the time of the flow reversal of the bore tip ($t = 5.7$ s). During this time water just before the bore tip sinks into the beach, resulting in a shoreline retreat. In other words for 1.3 s (between $t = 4.4$ s and $t = 5.7$ s) the shoreward flow direction behind the shoreline is combined with a seaward movement of the shoreline itself. This phenomenon is analysed in the simulation results of Steenhauer et al. (2012). In the backwash, the smaller volume of water on the permeable beach causes a slower shoreline retreat, compared to the impermeable counterpart. As a result the time it takes for the shoreline to be back at the initial shoreline location is approximately the same for both permeable beach (shorter shoreline excursion and slower retreat), and impermeable beach (longer excursion and faster retreat).

Because of the smaller infiltration discharge on the sand beach (compared to the gravel beach), the position of the shoreline movement remains similar to the impermeable beach for a longer period of time (1.2 s after bore arrival at the initial shoreline location). For the following 0.8 s of the swash event (from $t = 3.2$ s to 4.0 s), the rapid advance of the shoreline on the permeable beach is slightly greater than on the impermeable beach. This is due to the effect of infiltration on the velocity profile, especially in the region close to the bore tip. The infiltrating water is the water closest to the bed, and hence has the least forward momentum. The flow left on the beach has therefore a higher momentum, which causes the increase in the speed of propagation of the shoreline, compared to the impermeable beach. From $t = 4.0$ s onwards, the sand beach results show the same behaviour as the gravel beach results. The advance of the shoreline becomes slower than on the impermeable beach, and the shoreline reaches its maximum run-up before the flow at the shoreline changes direction. However these effects are less pronounced than for the gravel beach, since infiltration is smaller. The maximum run-up on the permeable beach is 4.3 m which is just 0.2 m or 4.3% less than on the impermeable beach. The flow reaches its maximum run-up after 5.2 s, approximately 0.4 s earlier than on the impermeable beach, and 0.4 s before flow reversal at the shoreline. In the backwash, the retreat of the shoreline on the permeable beach is faster than on the impermeable beach, even though the total volume of water on the beach at the start of the backwash is smaller (Fig. 4a). This is probably due to the infiltration just behind the shoreline which increases the speed of the shoreline retreat. Fig. 2 shows that the infiltration discharge during the final stages of backwash, after $t = 7.3$ s, is very close to zero. However, because of the very small flow depth, a very small volume of water that infiltrates into the beach has a significant influence on the shoreline position.

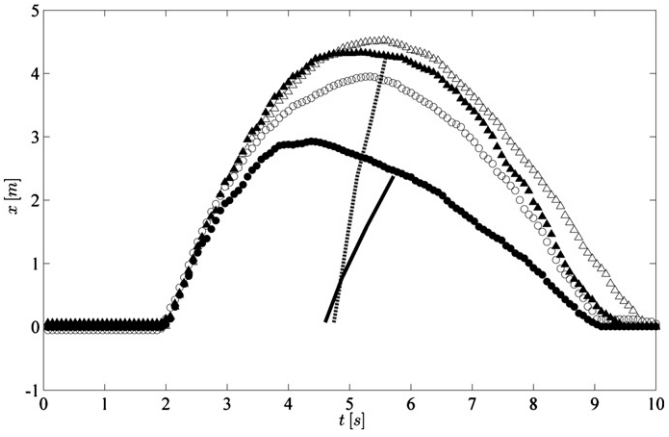

Fig. 3. Time series of shoreline position for sand (▲) and (●) gravel beaches. Time series of the flow reversal location for permeable sand (- -) and gravel (-) beaches. Shoreline positions for the corresponding impermeable beaches from Kikkert et al. (2012) are shown with open symbols.

3.3. Flow depth

Ensemble-averaged cross-shore flow depth profiles, $\overline{h}(x)$ (swash lenses) are presented in Fig. 4a for the sand beach and in Fig. 4b for the gravel beach, for six different times over the full swash cycle. On the gravel beach flow depths are affected by beach permeability soon after the bore arrival: water loss into the beach results in lower water depths in the region close to the bore tip, where infiltration rates are highest. From $t = 3.04$ s until the end of the uprush, the region of shallower depth (compared to the corresponding impermeable beach) extends, so that at around the time of maximum run-up it covers almost the entire beach. During the backwash the region of the beach significantly affected by infiltration shrinks. In this period infiltration is very small and the surface water is removed from the beach at a slower rate than from the impermeable beach. This slows down the rate of decrease of flow depths and brings them closer to the impermeable beach results at the lower end of the beach.

For the sand beach the infiltration discharges are much smaller than for the gravel beach, resulting in a more subtle effect of the permeability on the swash lens. During uprush the flow depths near the initial shoreline position ($x = 0.072$ m) are very similar for both the permeable and impermeable beaches. Further up the slope the flow depth is initially similar, but over time the slightly lower flow depth on the permeable beach becomes visible ($t = 4.08$ s). In the backwash the flow depths on the permeable beach are lower than on the impermeable beach further up the slope, but similar at the lower end of the beach.

The time series of $\overline{h}$ at several x-locations across the beach are presented in Fig. 5. In order to take into account the different times of bore arrival, t_{ba}, and flow reversal, t_{fr}, on the permeable and impermeable beaches, dimensionless time $t_* = (t - t_{ba}) / (t_{ba} - t_{fr})$ is introduced. (The values of t_{ba} and t_{fr} can be obtained from results presented in Figs. 3 and 6). As already shown, infiltration into the beach results in smaller surface water depths. This effect is more pronounced in the backwash than in the uprush, for the higher cross-shore locations compared to lower locations, and for the more permeable gravel beach. The influence of infiltration is hence most visible for the gravel beach at the locations further up the slope, especially in the backwash.

3.4. Velocity

Time series of depth-averaged ensemble-averaged bed-parallel velocities, $\langle\overline{u}\rangle$, generated from the simultaneous velocity and depth measurements, are shown in Fig. 6. The time series of velocity has similar overall features as those previously reported for impermeable beaches: upon bore arrival velocities suddenly increase and reach maximum; as the bore climbs the slope the flow decelerates at approximately constant rate; after flow reversal the velocity magnitude increases and reaches maximum; towards the end of the backwash the velocity magnitude decreases and becomes very small.

Using t_* as the time axis, the effect of infiltration into the bed is visible only in the backwash: on permeable beaches the backwash is

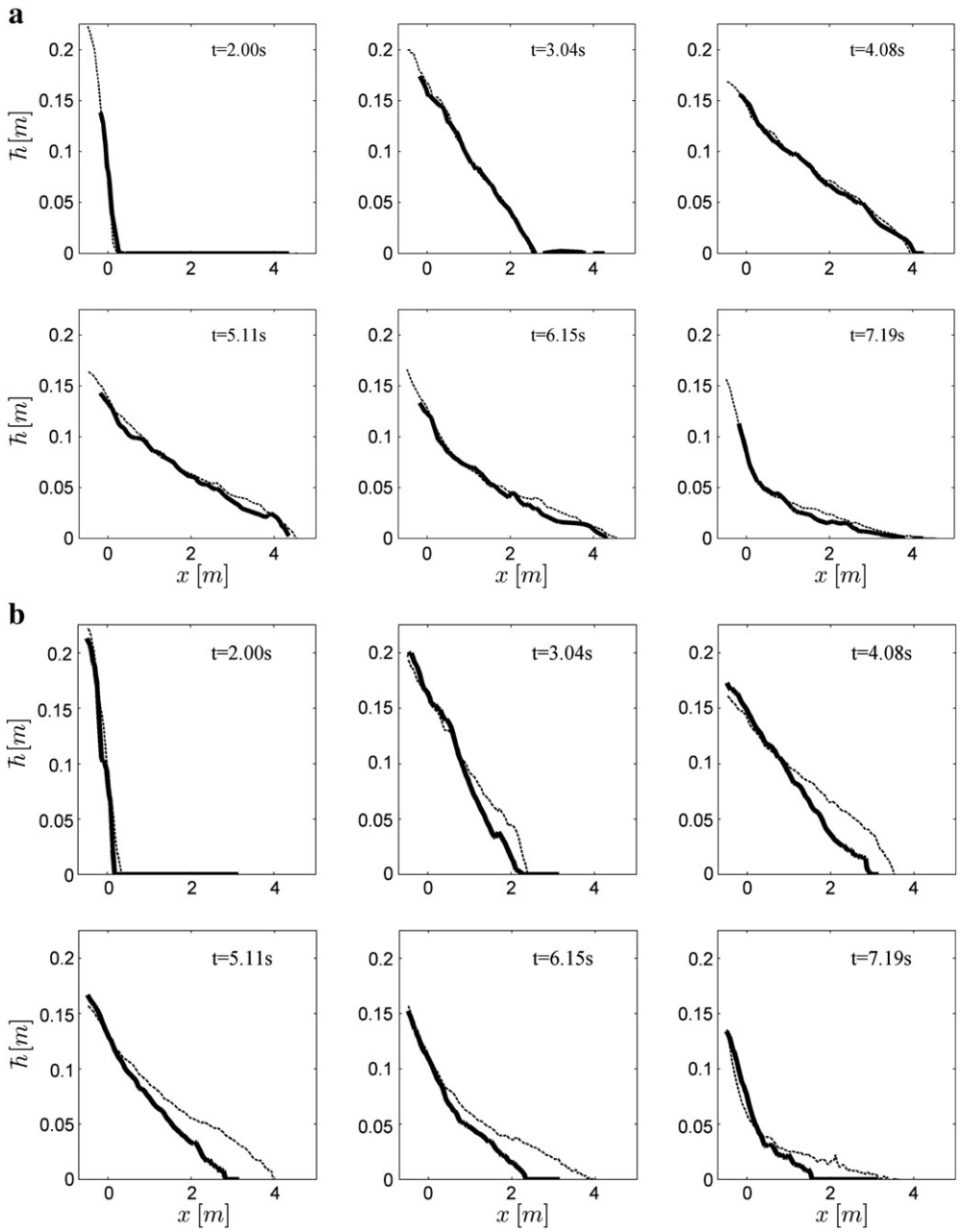

Fig. 4. a. Swash lenses at six times on the sand beach. Swash lenses on the corresponding impermeable sand beach from Kikkert et al. (2012) are shown with a dashed line. b. Swash lenses at six times on the gravel beach. Swash lenses on the corresponding impermeable gravel beach from Kikkert et al. (2012) are shown with a dashed line.

shorter and maximum backwash velocities are smaller than on impermeable beaches. The differences between velocity time series on permeable and impermeable beaches are much more pronounced for the gravel beach than for the sand beach, and they increase with distance up the slope. At $x = 2.377$ m on the gravel beach the maximum velocity in the backwash is lower for the permeable beach by 0.8 m/s and the duration of the backwash is almost zero. A possibility of having only an uprush phase in a swash event on a highly permeable beach has been highlighted in the numerical simulations of Steenhauer et al. (2012).

So far the comparison between impermeable and permeable beaches has shown significant differences in flow depths and velocities, especially at the locations further up the slope and in the backwash, where the effects of water loss due to infiltration are highest. These bulk effects make the comparison of the velocity profiles very difficult if not impossible. For this reason the ensemble-averaged velocity profiles are presented only for the permeable beaches (bed-parallel velocity in Fig. 7 and the bed-normal velocity in Fig. 8). Overall the velocity profiles show similar characteristics as profiles from the impermeable beach experiments (Kikkert et al., 2012). Near the initial shoreline position, the bed-parallel velocity profiles are very uniform during the uprush because the flow has very little time to develop a boundary layer. Flow first changes direction near the bed, where velocities are lowest, so that during the initial backwash the maximum velocity within the profile is near the bed, while the overall profile is again very uniform. During the late stages of the backwash, the increasing velocity and rapidly reducing flow depth result in very steep velocity gradients.

Comparison of the velocity profiles for different cross-shore locations shows that during the uprush the boundary layer becomes thinner for locations further up the slope. This is visible, for example, in the profiles for the gravel beach with a maximum velocity of ~1.5 m/s: the sharp change of the velocity gradient indicating the top of the boundary layer moves towards the bed as the x-location moves up the beach.

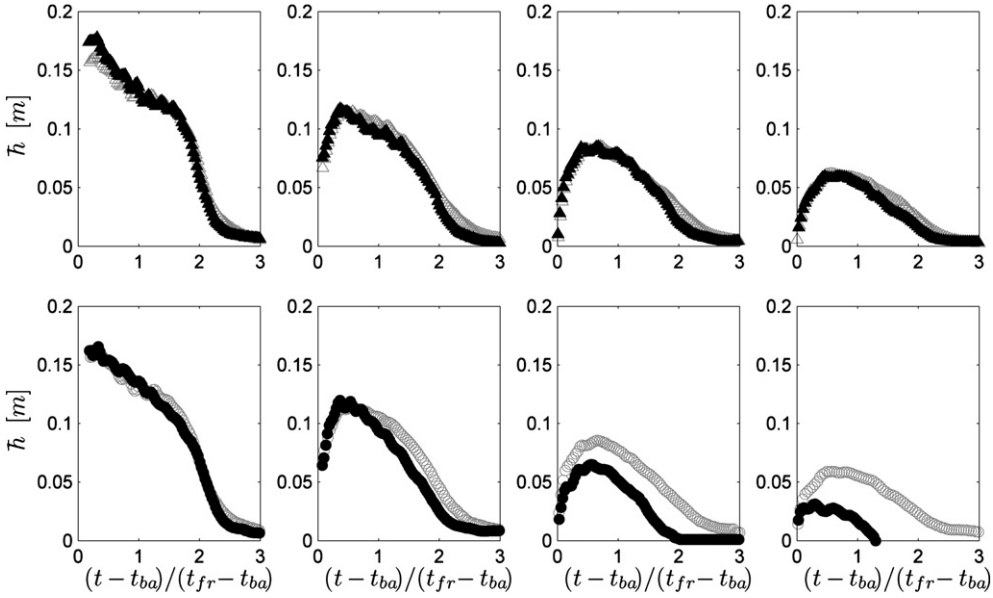

Fig. 5. Time series of $\overline{h}$ for the sand beach (▲, top panels) and for the gravel beach (●, bottom panels) at four locations (from left to right $x = 0.072$ m, 0.772 m, 1.567 m and 2.377 m). Time series for the corresponding impermeable beaches from Kikkert et al. (2012) are shown with open symbols.

This is opposite to the previously observed behaviour on rough impermeable slopes, where the boundary layer further up the slope becomes thicker because it has more time to develop. On permeable beaches infiltration into the bed has a stronger effect than the boundary layer development, hence resulting in thinner boundary layer at higher locations.

The bed-normal velocity profiles (Fig. 8) are uniform and close to zero for most of the swash event. Positive velocities related to the remaining circulation in flow after the dam break can be seen just after bore arrival. At the initial shoreline location velocities are positive again close to the end of the backwash, possibly because flow is approaching the horizontal bed section. Chen and Chiew (2007) recorded small negative bed-normal velocities near the bed in steady open channel flow with bed suction. In the present experiments negative velocities are recorded only for the gravel beach further up the slope ($x = 1.567$ m), however they extend uniformly throughout the flow column, probably due to the relatively high ratio of infiltration velocity to the bed-parallel velocity. For the sand beach this ratio of infiltration to maximum bed-parallel velocity is much smaller, and no negative vertical velocities were recorded.

To investigate the effect of the permeability on the velocity profiles and in particular the development of the boundary layer, the uniformity of the velocity profiles is expressed using the deviation of the profile from its depth-averaged value (O'Donoghue et al., 2010):

$$\beta = \left[\frac{1}{\overline{h}}\int_0^{\overline{h}}\left[\overline{u}(x,z,t)-\overline{\langle u\rangle}(x,t)\right]^2 dz\right]^{1/2}. \tag{2}$$

For a perfectly uniform profile β is zero, so the higher the value of β the less uniform is the velocity profile. The time series of β is presented in Fig. 9. Time is again non-dimensionalised using t_{ba} and t_{fr}. During

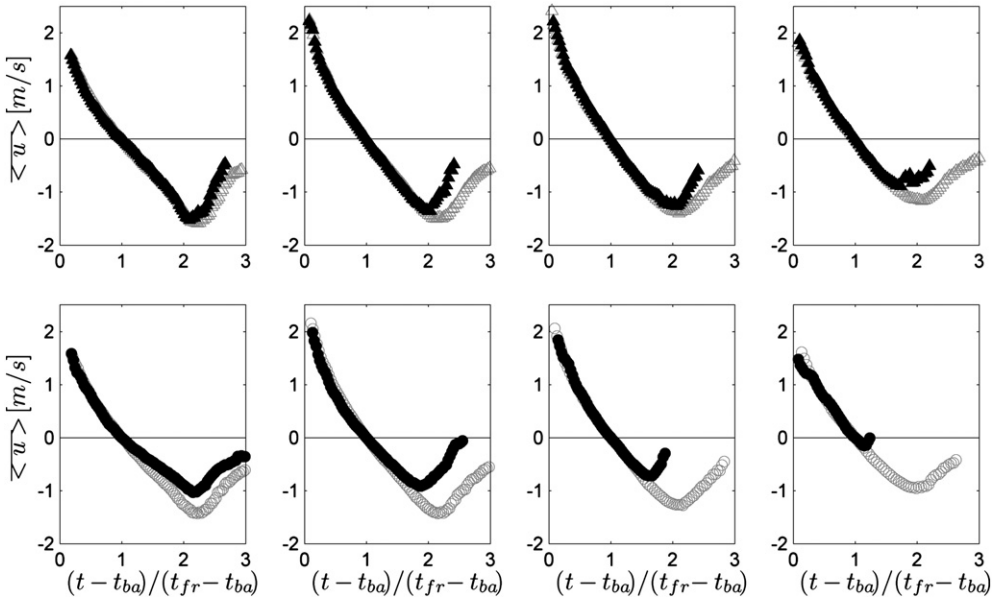

Fig. 6. Time series of $\overline{\langle u\rangle}$ for the sand beach (▲, top panels) and gravel beach (●, bottom panels) at four locations (from left to right $x = 0.072$ m, 0.772 m, 1.567 m and 2.377 m). Time series for the corresponding impermeable beaches from Kikkert et al. (2012) are shown with open symbols.

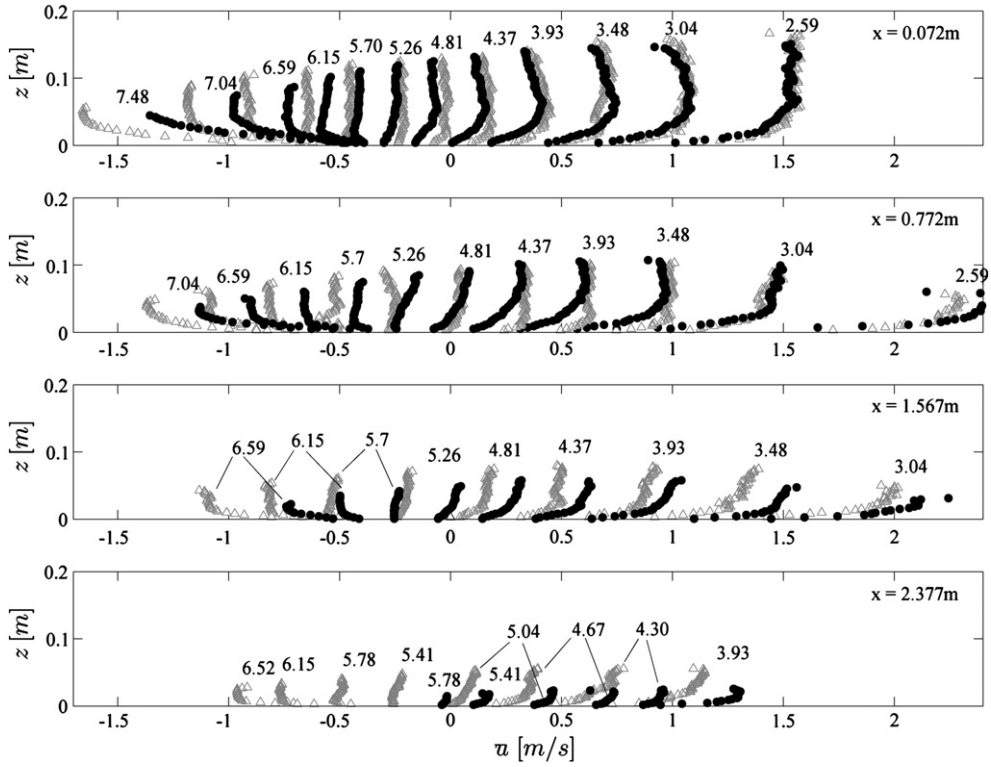

Fig. 7. Ensemble-averaged bed-parallel velocity profiles for the sand beach (Δ) and the gravel beach (●) at four locations. The number above the profile indicates time, t [s].

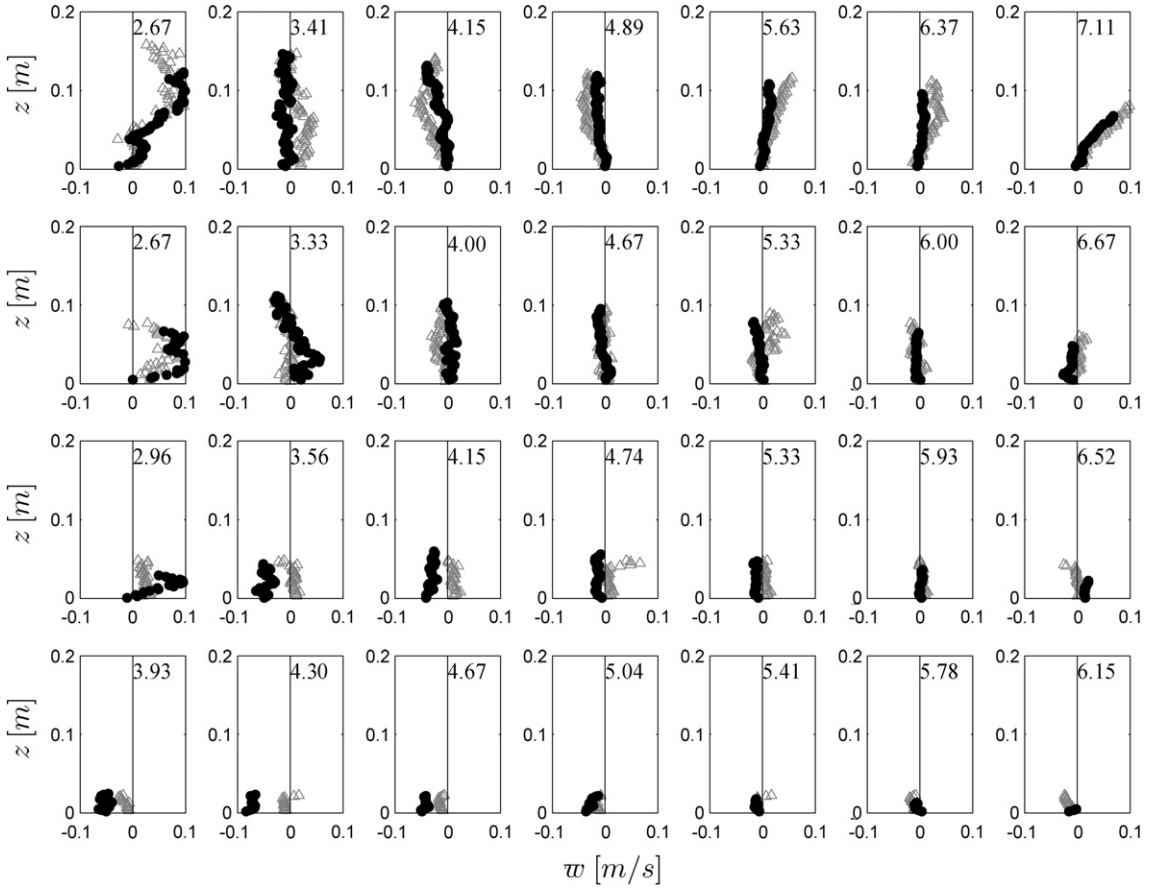

Fig. 8. Ensemble-averaged bed-normal velocity profiles for the sand beach (Δ) and the gravel beach (●) at four locations (from top to bottom $x = 0.072$ m, 0.772 m, 1.567 m and 2.377 m). The number above the profile indicates time, t [s].

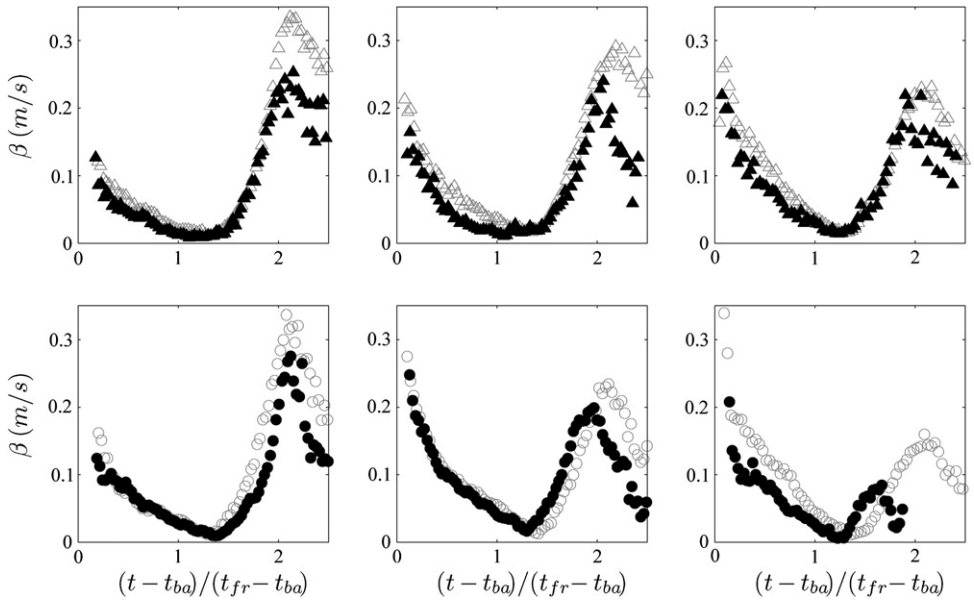

Fig. 9. Time series of β for the sand beach (▲, top) and for the gravel beach (●, bottom) at $x = 0.072$ m (left), $x = 0.772$ m (middle) and $x = 1.567$ m (right). Time series of β for the corresponding impermeable beaches from Kikkert et al. (2012) are shown with open symbols.

uprush the velocity profiles are somewhat more uniform for both permeable beaches than for their impermeable counterparts. This is consistent with the previous observation that during uprush the developing boundary layer sinks into the bed, and also agrees with experimental results obtained in open channel flows with suction (Chen and Chiew, 2004; Maclean, 1991). During the majority of the backwash, infiltration into the sand beach is practically zero, so the velocity profile uniformity for the permeable and impermeable beaches are practically identical: as the boundary layer develops the profile becomes progressively more non-uniform. In the final stages of the backwash the velocity magnitudes on the permeable beach are much lower than on the impermeable beach, resulting in much more uniform profiles. For the gravel beach the effect of infiltration during the early stages of the backwash varies between locations: at the higher locations the velocity profiles for the permeable beach are less uniform than for the impermeable beach, probably due to the smaller flow depth, but similar depth-averaged velocity, on the permeable beach. At the final stage of the backwash the depth-averaged velocity on the permeable gravel beach becomes very small, resulting again in more uniform velocity profiles, compared to the impermeable gravel beach.

3.5. Turbulence

Results for turbulence are presented only for the gravel beach, where the number of repeated runs of the swash event was sufficiently large to produce reliable estimates of turbulent stress and turbulent kinetic energy, *TKE*. *TKE* is here defined as $\overline{u'u'} + \overline{w'w'}$ where $u' = u - \overline{u}$ and w is the bed-normal velocity. *TKE* profiles are presented in Fig. 10. The overall characteristics are similar to those found for swash on the impermeable beaches (Kikkert et al., 2012). During early uprush turbulence generated by the collapse of the bore dominates, resulting in non-zero *TKE* profiles. High velocity gradients cause a peak in *TKE* close to the bed. With time *TKE* reduces throughout the flow column as turbulence dissipates and less turbulence is generated because of lower velocities. Only after the flow has spent a reasonable amount of time in the backwash are significant amounts of bed-generated turbulence produced again, resulting in an increase in *TKE* near the bed.

Time series of near-bed *TKE* (at $z = 10$ mm) for 4 x-locations are presented in Fig. 11, along with the results for the impermeable beach from Kikkert et al. (2012). Time is again non-dimensionalised using t_{ba} and t_{fr}. Near the initial shoreline location ($x = 0.072$ m) the results from the two beaches during the uprush are practically identical, confirming that *TKE* is predominantly bore-generated. Further up the slope, *TKE* on the permeable beach is lower than on the impermeable beach and this difference increases with distance up the slope. This is probably due to the effect of the near-bed *TKE* disappearing with the water into the permeable beach, also observed in open-channel flows with suction (Chen and Chiew, 2007; Lu et al., 2008). This is a cumulative effect which occurs while the bore is climbing the slope, so it is more pronounced at higher locations. Furthermore, locations further up the slope have high values of infiltration rates for longer, because it takes a longer time for the infiltrated water to saturate the whole beach profile. At the beginning of the backwash (non-dimensional time = 1), *TKE* production is small, so the comparison of *TKE* shows similar results as during the uprush. For locations further up the slope the backwash on the permeable beach is very short, so the intense generation of turbulence does not start. For lower locations the rate of increase in TKE in the later stages of the backwash on the permeable and impermeable beach is similar. Velocity and acceleration are lower on the permeable beach but the boundary layer is probably thinner, hence resulting in similar velocity gradients and similar TKE production.

Profiles of turbulent shear stress, $-\overline{u'w'}$, are presented in Fig. 12. Just after bore arrival, $-\overline{u'w'}$ is zero away from the bed where the gradient of the velocity profile is very small. Close to the bed, the turbulent shear stress is non-zero as the flow develops the boundary layer. Over time, the influence of the bed-generated turbulent shear stress is seen to move higher up in the water column; however the overall magnitude of the turbulent shear stress is decreasing because of the decreasing velocity. By the time of flow reversal the profiles are uniform and zero. The steep velocity gradients around the time of maximum backwash velocity are reflected by a small increase in the magnitude of turbulent shear stress. The near bed ($z = 10$ mm) comparison of the absolute turbulent shear stress, presented in Fig. 13, shows similar results as the near bed *TKE*. During uprush, the results for the permeable and impermeable beaches are similar near the initial shoreline, whereas further up the slope, the turbulent shear stress

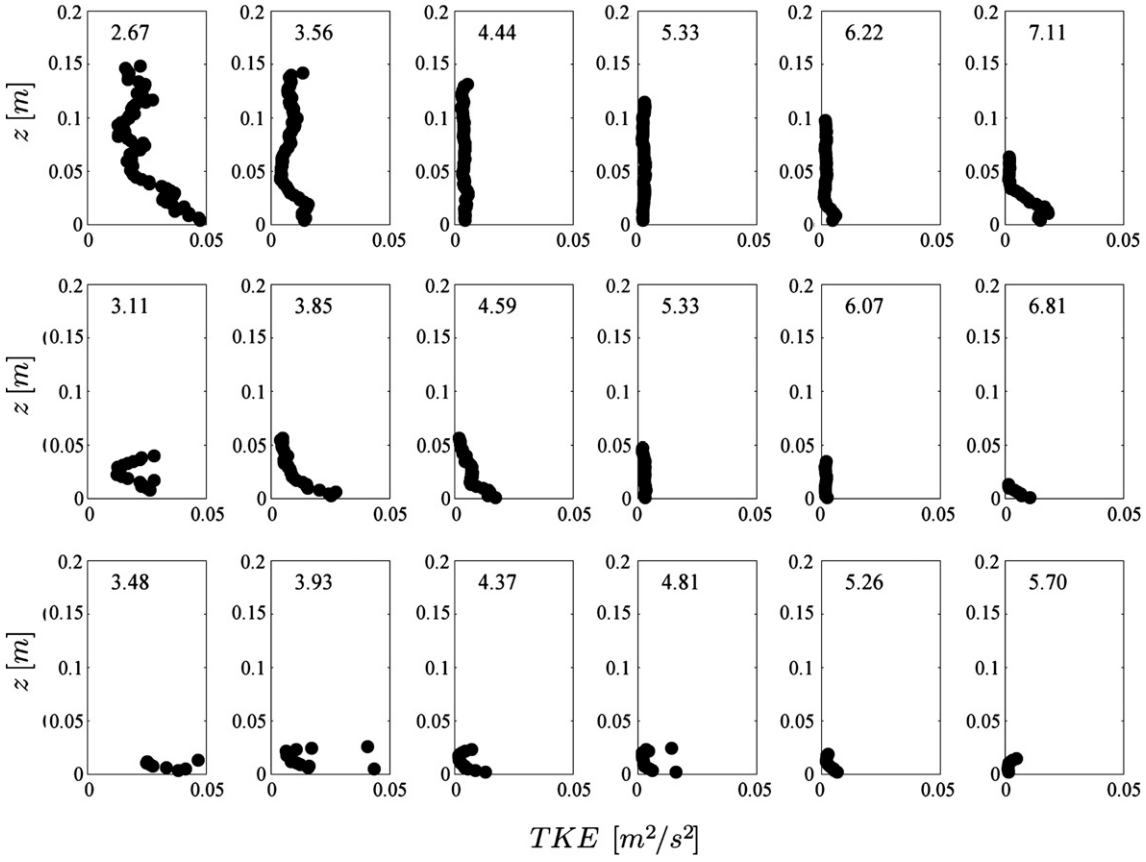

Fig. 10. Ensemble-averaged *TKE* profiles for the gravel beach at three locations (from top to bottom $x = 0.072$ m, 1.567 m and 2.377 m). The number above the profile indicates time, t [s].

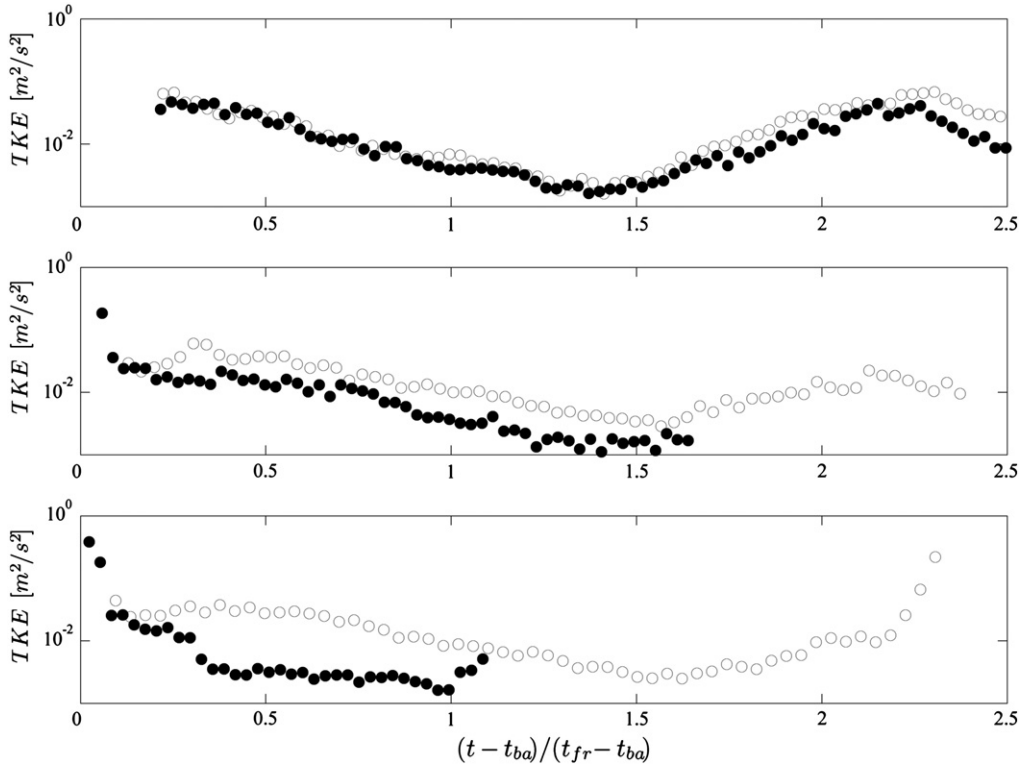

Fig. 11. Time series of near bed ($z = 10$ mm) turbulent kinetic energy for the gravel beach (●) at three locations (from top to bottom $x = 0.072$ m, 1.567 m and 2.377 m). Time series for the corresponding impermeable gravel beach from Kikkert et al. (2012) are shown with open symbols.

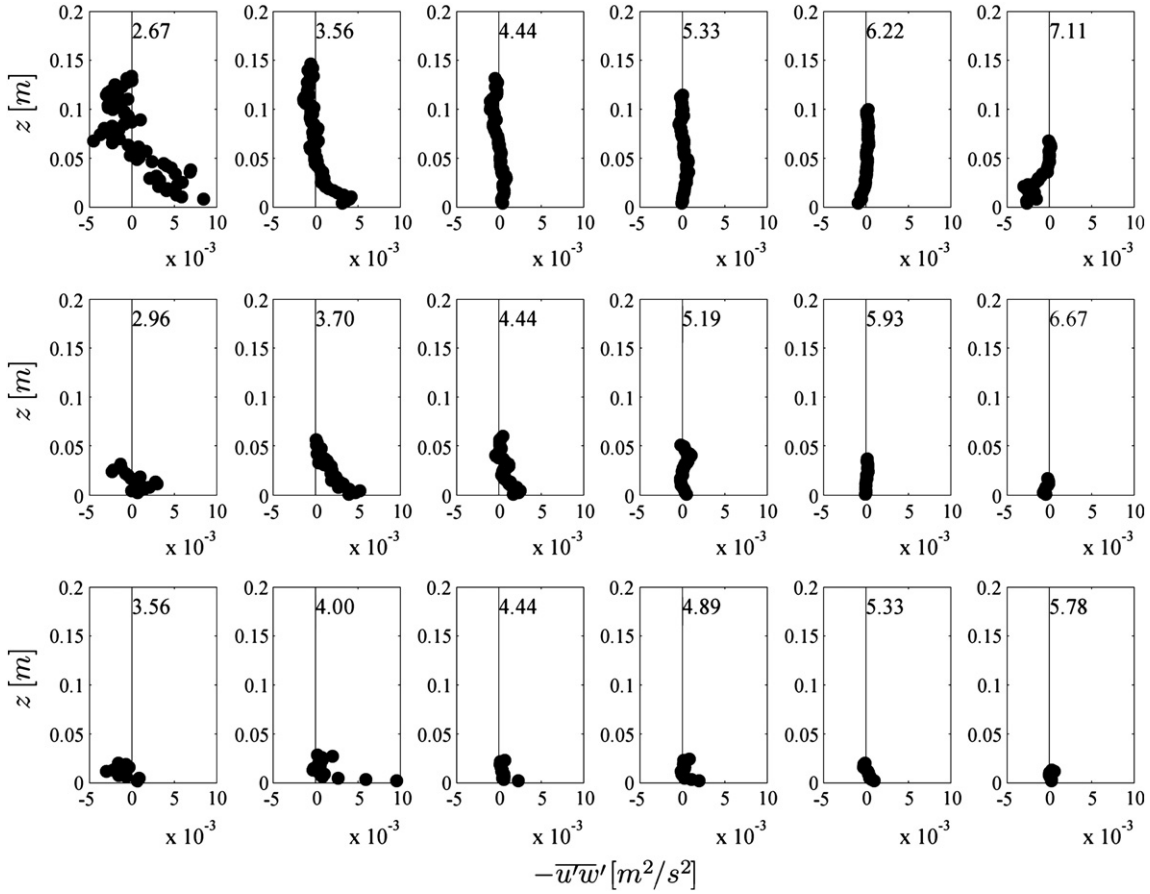

Fig. 12. Profiles of $-\overline{u'w'}$ for the gravel beach at three locations (from top to bottom $x = 0.072$ m, 1.567 m and 2.377 m). The number above the profile indicates time, t [s].

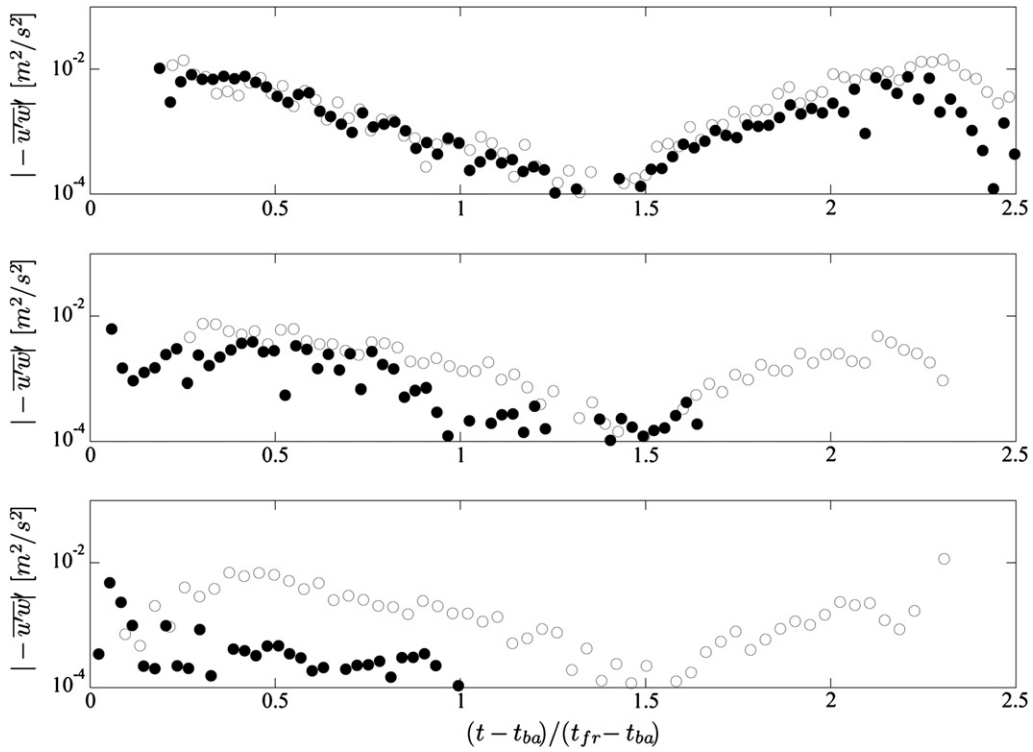

Fig. 13. Time series of near bed ($z = 10$ mm) $\left|-\overline{u'w'}\right|$ for the gravel beach (●) at, from top to bottom, $x = 0.072$ m, 1.567 m and 2.377 m. Time series for the corresponding impermeable gravel beach from Kikkert et al. (2012) are shown with open symbols.

is lower on the permeable beach. In the backwash the results are again similar near the initial shoreline position while further up the slope the turbulent shear stress remains very small due to the short duration of the backwash.

3.6. Bed shear stress

The traditional log-law is commonly used to estimate bed shear stress in steady uniform boundary layer flow over an impervious bed by fitting the log-law to the bed-parallel velocity profile. Kikkert et al. (2009, 2012) used the velocity measurements on rough impermeable slopes to estimate the shear stress in the swash zone using both log-law approach and the momentum balance method, where the bed shear stress is directly obtained from evaluating the terms in the Depth-Integrated Reynolds-Averaged Navier–Stokes equations. Even though the flow in the swash zone is unsteady and non-uniform the results from the log-law approach were in good agreement with the results from the momentum balance. To enable the log-law approach to be used for a permeable bed the log law has to be modified (Maclean, 1991; Prinos, 1995). Chen and Chiew (2004) proposed the following modified log law:

$$\frac{\overline{u}-u_0}{u_*}=\frac{1}{\kappa}\ln\frac{z+z_0}{z_0}+\frac{w_0}{4u_*}\left(\frac{1}{\kappa}\ln\frac{z+z_0}{z_0}\right)^2 \tag{3}$$

where u_* is the shear velocity defined as $u_*=\sqrt{\tau_0/\rho}$ (τ_0 = bed shear stress, ρ = fluid density), u_0 is bed-parallel velocity at the beach surface, w_0 is bed-normal velocity at the beach surface (infiltration velocity), z_0 is the vertical displacement of the origin of the mean velocity profile and κ is the von Karman constant (=0.4). The infiltration velocities for the current experiments are obtained from the wetting front measurements of Steenhauer et al. (2011), assuming that the infiltration velocity at the wetting front is the same as at the beach surface. No wetting front measurements were obtained for the first 1100 mm up the slope, therefore the modified log law could only be applied at x = 1.567 m and 2.377 m. To fit the data to the modified log law and obtain the shear velocity, Chen and Chiew (2004) rewrote Eq. (3) as

$$\overline{u}=ax^2+bx+c \tag{4}$$

where $x=\frac{1}{\kappa}\ln\left(\frac{z+z_0}{z_0}\right)$, $a=\frac{w_0}{4}$, $b=u_*$, $c=u_0$.

Values for z_0, u_* and u_0 were obtained by fitting the second order polynomial to the experimental data using a trial-and-error routine that maximised the number of data points included in the fit and ensured the determined value for w_0 matched the measured value. The shear velocities obtained from the iterative process are used in further analysis and compared with those from the classical log law in Fig. 14. For both beaches the difference between the two methods is consistent: the modified log law gives higher estimates of the shear velocity than the classical log law and the difference increases with increasing infiltration velocities. For the sand beach the difference was sufficiently small to justify using only estimates of shear velocity obtained from the classical log law, but bearing in mind it may be slightly underestimated. For the gravel beach the estimates for the shear velocity using the modified log law are significantly higher than using the classical log law, especially at the beginning of the uprush (Fig. 14). For this reason the classical log law should not be used while infiltration rates are significant, i.e., between bore arrival and the time of saturation of a beach at a particular x location. The time from bore arrival until saturation is determined from the wetting front measurements or estimated using the average infiltration velocity from the wetting front measurements and the distance from the beach surface to the groundwater level, giving values of 0.055 s and 0.38 s at x = 0.072 m and 0.772 m respectively. After saturation the infiltration velocity reduces rapidly (Steenhauer et al., 2011). It is assumed that during this time the infiltration velocity is sufficiently low to justify using the classical log law method to obtain estimates for the bed shear stress. Besides the method used for obtaining the bed shear stress estimates, the accuracy of these estimates depends on the accuracy of the velocity data. Because of the greater number of repeat experiments on the gravel beach, the velocity profiles are smoother than the profiles for the sand beach (Fig. 7) and hence

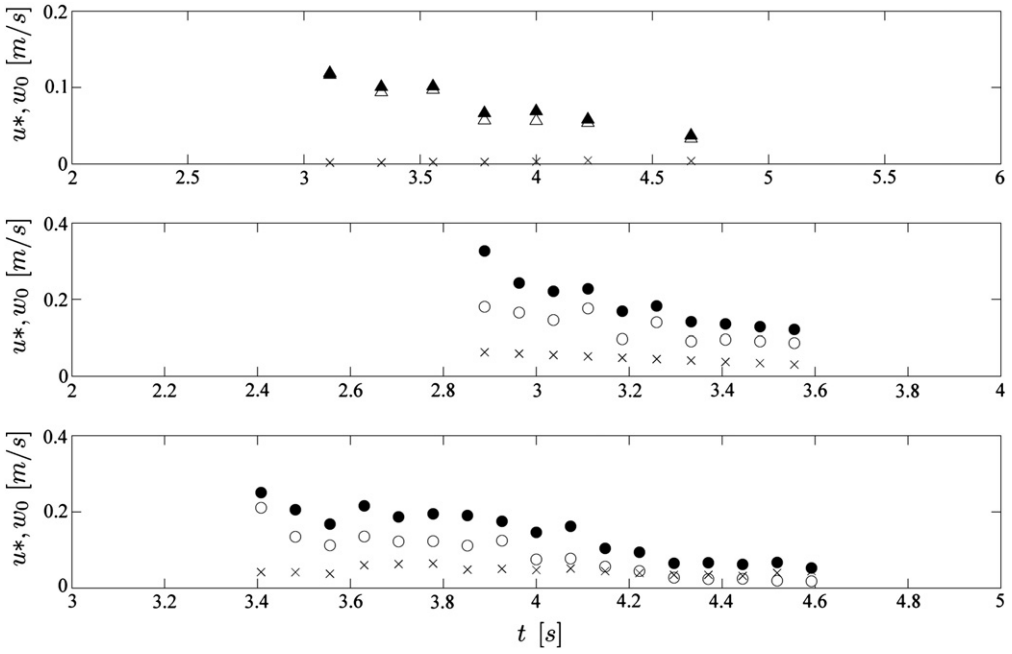

Fig. 14. Time series of shear velocity estimated using the log law (Δ and ○) and modified log law (▲ and ●), and infiltration velocity (x) for sand beach at x = 1.567 m (top panel), gravel beach at x = 1.567 m (middle panel) and gravel beach at x = 2.377 m (bottom panel).

bed shear stress estimates (Figs. 15 and 16) are more accurate. However, the accuracy of the estimates on the sand beach is still considered acceptable for a comparison with the bed shear stress on the corresponding impermeable beach and for the observation of the general trends.

The time series of bed shear stress estimates for the sand and gravel beaches are shown in Figs. 15 and 16 respectively. The overall shape of the bed shear stress time series for the permeable beaches is similar to previously reported results for the impermeable beaches (Kikkert et al., 2012): the magnitude of the bed shear stress changes in a similar way as the depth-averaged velocity; maximum values are seen at the beginning of the uprush, they gradually decrease to become very small around flow reversal, and in the backwash they increase again as the flow accelerates.

As expected the differences between the bed shear stress on the permeable and the impermeable beaches are more pronounced for the gravel beach (Fig. 16) than for the sand beach (Fig. 15). It is known from the literature that infiltration/exfiltration influences the bed shear stress in two ways: (i) directly, by changing the boundary layer thickness, and hence the shear stress; (ii) indirectly, by modifying the volume of water in the surface flow and hence also changing important terms in the momentum balance. Baldock and Nielsen (2010) call the latter mechanism 'continuity effect'. In steady-uniform flows the continuity effect is much smaller than the direct effect (Francalanci et al., 2008) and hence infiltration always increases bed shear stress (Chen and Chiew, 2004; Maclean, 1991). Similar results were obtained for an oscillatory flow with suction in a tunnel (Conley and Inman, 1994). For non-uniform flows the relative importance of the two effects depends on the particular flow conditions and they may act in the opposite directions, i.e., one enhancing and one decreasing the bed shear stress.

In our experiments the relative importance of the two mechanisms changes throughout the swash event. Consider first the gravel beach. The direct effect of infiltration into the beach dominates during the early uprush, resulting in a higher bed shear stress than on the impermeable counterpart. During later stages of the uprush the infiltration rates become smaller so the difference between the bed shear stress on permeable and impermeable beach gradually diminishes. Around the time of flow reversal the continuity effect kicks in and soon becomes predominant, due to the significant cumulative loss of water in the surface flow. For the locations further up the slope the continuity effect enhances shear stress, because the velocities on the permeable and impermeable beaches are similar (Fig. 6), but the flow depth is smaller (Fig. 5), resulting in steeper velocity gradients (Fig. 9). At the lowest position on the beach, however, the continuity effect results in a decreased bed shear stress on the permeable beach, because not only flow depths but also flow velocities are reduced.

For the sand beach (Fig. 15), the uprush bed shear stress at the lower locations is slightly smaller for the permeable beach than for its impermeable counterpart. This may be due to the evaluation method, which underestimates the magnitude of the bed shear stress. However, it can also be explained as a direct effect of exfiltration, which indeed occurs at these locations throughout most of the swash event. Exfiltration (i.e., injection) has been shown to decrease bed shear stress in steady open channel flows (Cheng and Chiew, 1998, 1999; Francalanci et al., 2008) and oscillatory flows (Conley and Inman, 1994). For locations further up the slope the direct effect of infiltration causes small increases in the permeable beach bed shear stress. In the backwash the differences between permeable and impermeable beaches are similar to those on the gravel beach, just much smaller. It is interesting to compare Fig. 16 with Fig. 13 for locations further up the beach: although the turbulent shear stress is much smaller on the permeable beach than on its impermeable counterpart, bed shear stresses are very similar. This means that for the permeable beach momentum transfer near the bed occurs not only

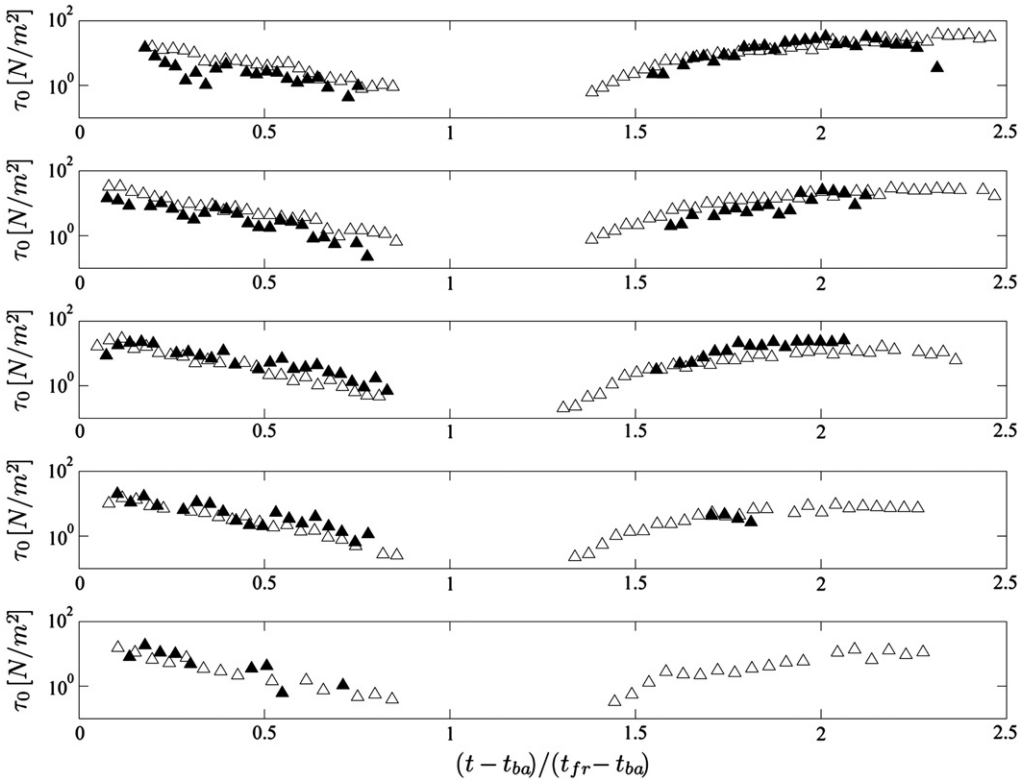

Fig. 15. Absolute bed shear stress time series for the sand beach (▲) at $x = 0.072$ m, $x = 0.772$ m, 1.567 m, 2.377 m and $x = 3.177$ m. Time series for the corresponding impermeable sand beach from Kikkert et al. (2012) are shown with open symbols.

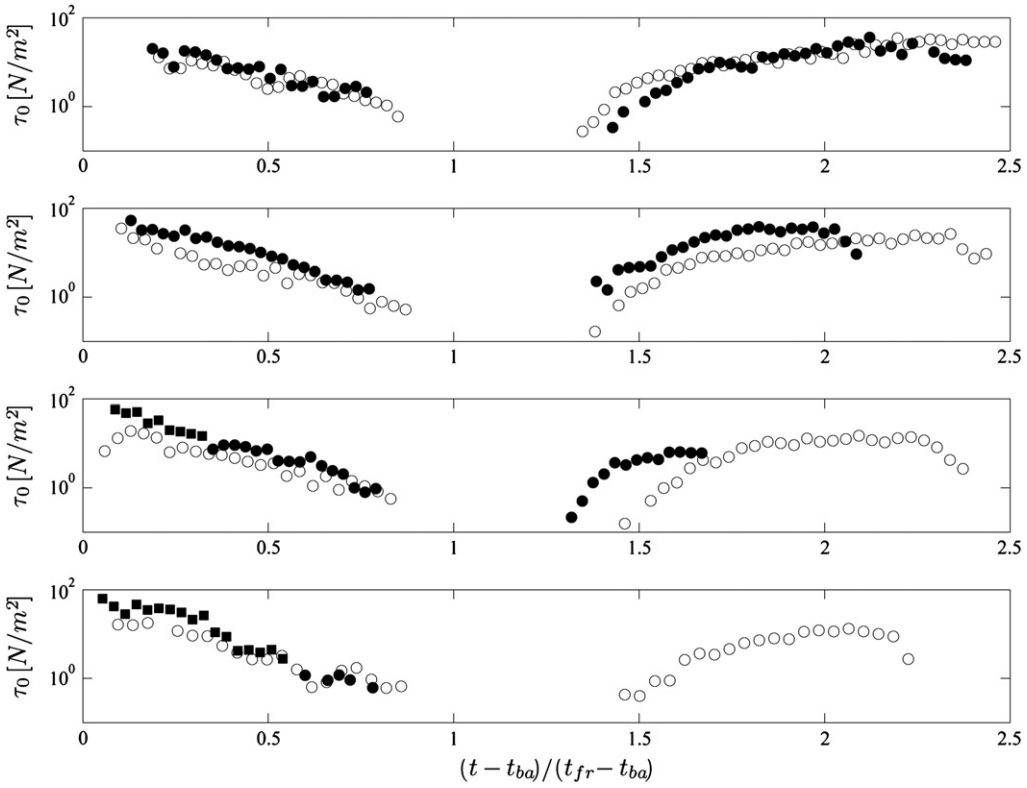

Fig. 16. Absolute bed shear stress time series for the gravel beach using log law (●) and modified log law (■) methods at $x = 0.072$ m, $x = 0.772$ m, 1.567 m and 2.377 m. Time series for the corresponding impermeable gravel beach from Kikkert et al. (2012) obtained using log law are shown with open symbols.

via turbulent motions, but also via other mechanisms such as transfer of bed-parallel velocity by the bed-normal velocity, and, perhaps, form-induced stress (Nikora et al., 2001).

A quadratic resistance law is often employed to parameterise shear stress in depth-averaged momentum balance equations. The resistance law can be written as

$$\tau_0 = c_f \rho \langle \overline{u} \rangle^2 / 2 \tag{5}$$

where ρ is the density and c_f the friction factor. The friction factor time series for the sand and gravel beaches are presented in Figs. 17 and 18, respectively. The overall behaviour of friction factors is very similar to the previously reported results for impermeable beaches of Kikkert et al. (2012), who showed that c_f is not just a function of the Reynolds number and relative roughness, but also depends on the boundary layer development and flow acceleration/deceleration. During the initial uprush the friction factors on the impermeable beaches were higher than values based on a steady uniform flow formula, because the incoming bore had little structure and the boundary layer developed while the bore travelled up the slope. The friction factors on the permeable beaches during the uprush are higher again, with the greatest difference at those locations where infiltration effects were greatest, because infiltration into the beach slows down the development of the boundary layer.

4. Conclusions

A detailed experimental investigation has been carried out to investigate the effect of permeability on the hydrodynamics of dam-break generated bores on steep coarse-grained beaches. Simultaneous measurements of the flow depth and velocity were obtained on two 1:10 permeable, but immobile beaches constructed from different size sediments. The finer sediment, sand, was an order of magnitude less permeable than the coarser sediment, gravel. The effect of the permeability on the hydrodynamics was evaluated by comparing the new results with previously published experimental results obtained on impermeable beaches with identical surface roughness. The experimental data yielded the following conclusions:

- During a swash cycle 33% and 52% of the surface water infiltrated into the coarse sand and gravel beach respectively. Infiltration rates were highest very soon after bore arrival on the beach, then gradually decreased to become very close to zero in the backwash.
- Due to the water loss the maximum run-up for the permeable beach is shorter than for the corresponding impermeable beach (3.0 m compared to 4.0 m for the gravel beach, and 4.3 m compared to 4.5 m for the sand beach). Throughout the backwash infiltration close to the shoreline has a significant effect on the shoreline position: the shoreline starts to retreat immediately after reaching the maximum run-up although the shoreward flow near the shoreline continues for quite a while; on the sand beach the shoreline retreats faster for the permeable beach than for its impermeable counterpart, even though the driving force (gravity) is smaller.
- Backwash depth-averaged velocities are significantly lower on the permeable beach compared to its impermeable counterpart because of the reduced volume of water in the surface flow.
- Velocity profiles on the permeable beaches indicate that, due to infiltration, the boundary layer sinks into the subsurface.
- The profiles of TKE and turbulent shear stress over permeable beaches show a very similar overall behaviour to that over impermeable beaches. However, turbulence intensity and turbulent shear stress are lower in the case of the permeable beaches because of the sinking of the lower end of the boundary layer into the beach.
- Despite reduced turbulence near the bed, bed shear stress and friction factor are enhanced for the permeable beaches compared to their impermeable counterparts. In the uprush the enhancement is due to the direct effect of infiltration (thinning of the boundary layer), whereas after the flow reversal the continuity effect (loss of water from the

surface flow) becomes predominant. On the sand beach exfiltration occurs close to the initial shoreline, which likely reduces the bed shear stress.

- Data from the present experiments can be used to test and develop models of bore-driven swash on permeable slopes. The detailed data are available on request from the authors.

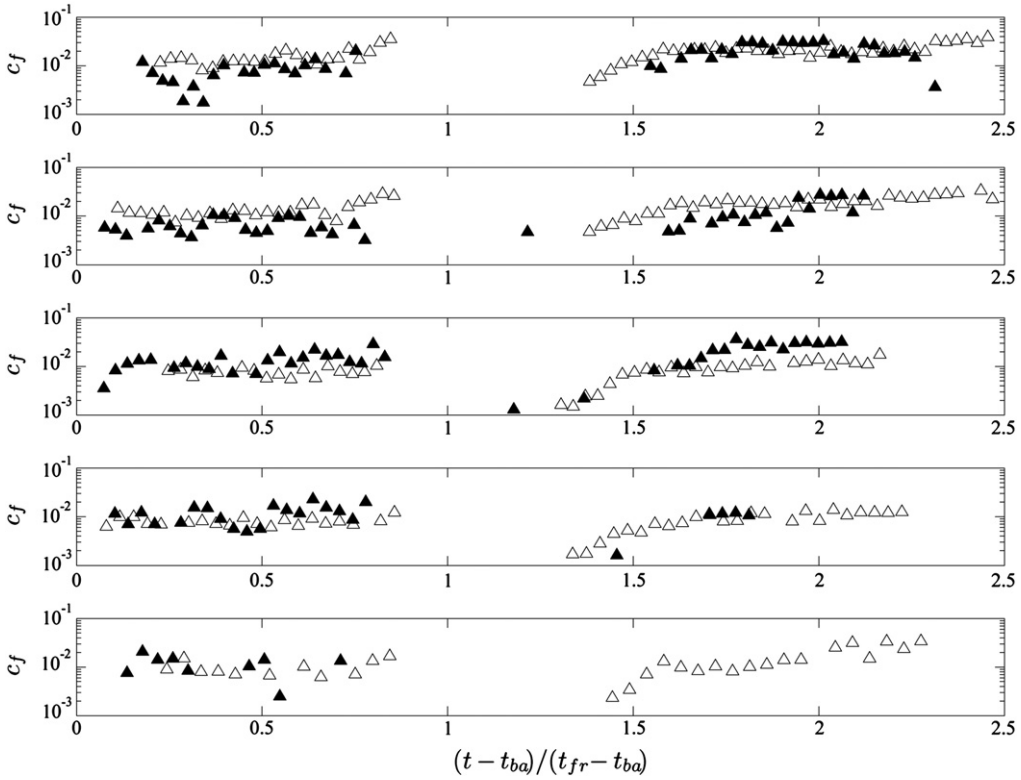

Fig. 17. Friction factor time series for the sand beaches (▲) at $x = 0.072$ m, $x = 0.772$ m, 1.567 m, 2.377 m and $x = 3.177$ m. Time series for the corresponding impermeable sand beach from Kikkert et al. (2012) are shown with open symbols.

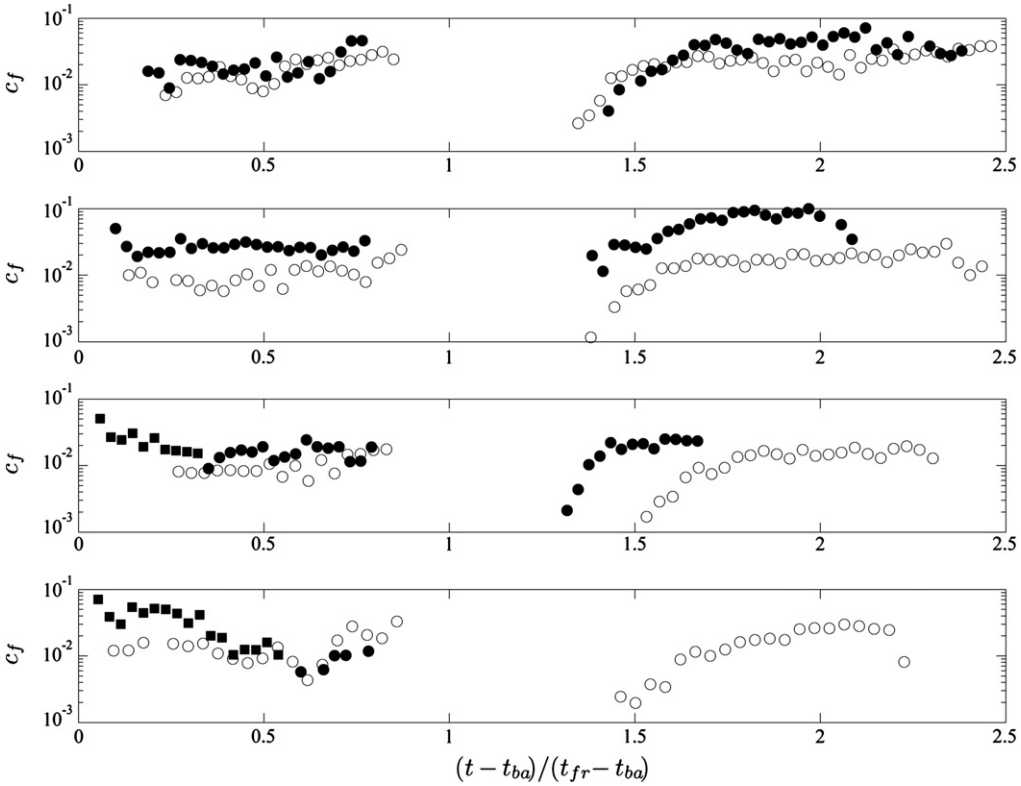

Fig. 18. Friction factor time series for the gravel beach using log law (●) and modified log law (■) methods at x = 0.072 m, x = 0.772 m, 1.567 m and 2.377 m. Time series for the corresponding impermeable gravel beach from Kikkert et al. (2012) obtained using log law are shown with open symbols.

Acknowledgements

This work was funded by the UK EPSRC via research grant EP/E011330/1.

References

Austin, M.J., Masselink, G., 2006. Observations of morphological change and sediment transport on a steep gravel beach. Marine Geology 229, 59–77.
Baldock, T.E., Hughes, M.G., 2006. Field observations of instantaneous water slopes and horizontal pressure gradients in the swash-zone. Continental Shelf Research 26, 574–588.
Baldock, T.E., Nielsen, P., 2010. Discussion of "effect of seepage-induced nonhydrostatic pressure distribution on bed-load transport and bed morphodynamics" by Simona Francalanci, Gary Parker, and Luca Solari. Journal of Hydraulic Engineering 136, 77–79.
Barnes, M.P., O'Donoghue, T., Alsina, J.M., Baldock, T.E., 2009. Direct bed shear stress measurements in bore-driven swash. Coastal Engineering 56, 853–867.
Blenkinsopp, C.E., Turner, I.L., Masselink, G., Russell, P.E., 2011. Swash zone sediment fluxes: field observations. Coastal Engineering 58, 28–44.
Butt, T., Russell, P., 2000. Hydrodynamics and cross-shore sediment transport in the swash-zone of natural beaches: a review. Journal of Coastal Research 16, 255–268.
Chen, X., Chiew, Y.-, 2004. Velocity distribution of turbulent open-channel flow with bed suction. Journal of Hydraulic Engineering 130, 140–148.
Chen, Z., Chiew, Y.-, 2007. Turbulence characteristics of open-channel flow with bed suction. Journal of Engineering Mechanics 133, 1388–1393.
Cheng, N.-, Chiew, Y.-, 1998. Turbulent open-channel flow with upward seepage. Journal of Hydraulic Research 36, 415–431.
Cheng, N.-, Chiew, Y.-, 1999. Incipient sediment motion with upward seepage. Journal of Hydraulic Research 37, 665–681.
Conley, D.C., Griffin Jr., J.G., 2004. Direct measurements of bed stress under swash in the field. Journal of Geophysical Research C: Oceans 109 (C03050), 1–12.
Conley, D.C., Inman, D.L., 1994. Ventilated oscillatory boundary layers. Journal of Fluid Mechanics 273, 261–284.
Elfrink, B., Baldock, T., 2002. Hydrodynamics and sediment transport in the swash zone: a review and perspectives. Coastal Engineering 45, 149–167.
Francalanci, S., Parker, G., Solari, L., 2008. Effect of seepage-induced nonhydrostatic pressure distribution on bed-load transport and bed morphodynamics. Journal of Hydraulic Engineering 134, 378–389.
Horn, D.P., Mason, T., 1994. Swash zone sediment transport modes. Marine Geology 120, 309–325.
Hughes, M.G., 1992. Application of a non-linear shallow water theory to swash following bore collapse on a sandy beach. Journal of Coastal Research 8, 562–578.
Hughes, M.G., Masselink, G., Brander, R.W., 1997. Flow velocity and sediment transport in the swash zone of a steep beach. Marine Geology 138, 91–103.
Kikkert, G.A., Pokrajac, D., O'Donoghue, T., 2009. Bed-shear stress in bore-generated swash on steep beaches. Proceedings of 6th International Conference on Coastal Dynamics.
Kikkert, G.A., O'Donoghue, T., Pokrajac, D., Dodd, N., 2012. Experimental study of bore-driven swash hydrodynamics on impermeable rough slopes. Coastal Engineering 60, 149–166.
Lara, J.L., Losada, I.J., Liu, P.L.-, 2006. Breaking waves over a mild gravel slope: experimental and numerical analysis. Journal of Geophysical Research C: Oceans 111.
Lu, Y., Chiew, Y.-, Cheng, N.-, 2008. Review of seepage effects on turbulent open-channel flow and sediment entrainment. Journal of Hydraulic Research 46, 476–488.
Maclean, A.G., 1991. Open channel velocity profiles over a zone of rapid infiltration. Journal of Hydraulic Research 29, 15–27.
Masselink, G., Hughes, M., 1998. Field investigation of sediment transport in the swash zone. Continental Shelf Research 18, 1179–1199.
Masselink, G., Puleo, J.A., 2006. Swash-zone morphodynamics. Continental Shelf Research 26, 661–680.
Masselink, G., Russell, P., 2006. Flow velocities, sediment transport and morphological change in the swash zone of two contrasting beaches. Marine Geology 227, 227–240.
Masselink, G., Russell, P., Blenkinsopp, C., Turner, I., 2010. Swash zone sediment transport, step dynamics and morphological response on a gravel beach. Marine Geology 274, 50–68.
Nikora, V., Goring, D., McEwan, I., Griffith, G., 2001. Spatially averaged open-channel flow over rough bed. Journal of Hydraulic Engineering 127, 123–133.
O'Donoghue, T., Pokrajac, D., Hondebrink, L.J., 2010. Laboratory and numerical study of dambreak-generated swash on impermeable slopes. Coastal Engineering 57, 513–530.
Pedrozo-Acuña, A., Simmonds, D.J., Otta, A.K., Chadwick, A.J., 2006. On the cross-shore profile change of gravel beaches. Coastal Engineering 53, 335–347.
Petti, M., Longo, S., 2001. Turbulence experiments in the swash zone. Coastal Engineering 43, 1–24.
Prinos, P., 1995. Bed-suction effects on structure of turbulent open-channel flow. Journal of Hydraulic Engineering ASCE 121, 404–412.
Puleo, J.A., Beach, R.A., Holman, R.A., Allen, J.S., 2000. Swash zone sediment suspension and transport and the importance of bore-generated turbulence. Journal of Geophysical Research C: Oceans 105, 17021–17044.
Raubenheimer, B., 2002. Observations and predictions of fluid velocities in the surf and swash zones. Journal of Geophysical Research C: Oceans 107, 11-1–11-7.
Shin, S., Cox, D., 2006. Laboratory observations of inner surf and swash-zone hydrodynamics on a steep slope. Continental Shelf Research 26, 561–573.
Stansby, P.K., Chegini, A., Barnes, T.C.D., 1998. The initial stages of dam-break flow. Journal of Fluid Mechanics 374, 407–424.
Steenhauer, K., Pokrajac, D., O'Donoghue, T., Kikkert, G.A., 2011. Subsurface processes generated by bore-driven swash on coarse-grained beaches. Journal of Geophysical Research C: Oceans 116, C04013.
Steenhauer, K., Pokrajac, D., O'Donoghue, T., 2012. Implementation of ADER scheme for a bore on an unsaturated permeable slope. International Journal for Numerical Methods in Fluids 70, 682–702.
Sue, L., Nokes, R., Walter, R., 2006. Experimental modeling of tsunami generated by underwater landslides. Science of Tsunami Hazards 24, 267–287.